ACS OMEGA

Article

Cite This: ACS Omega 2019, 4, 19279−19286

http://pubs.acs.org/journal/acsodf

High-Yield Continuous-Flow Synthesis of Spheroidal C_{60}@Graphene Composites as Supercapacitors

Ibrahim K. Alsulam,[†,∥] Thaar M. D. Alharbi,[†,§,∥] Mahmoud Moussa,[‡,⊥] and Colin L. Raston*[,†]

[†]Flinders Institute for Nanoscale Science and Technology, College of Science and Engineering, Flinders University, Adelaide SA 5001, Australia

[§]Physics Department, Faculty of Science, Taibah University, Al Madinah Al Munawwarah 42353, Saudi Arabia

[‡]School of Chemical Engineering, The University of Adelaide, Adelaide SA 5001, Australia

[⊥]Department of Chemistry, Faculty of Science, Beni-Suef University, Beni-Suef 62111, Egypt

Supporting Information

ABSTRACT: Graphene spheres confining fullerene C_{60} are quantitatively formed under high-shear and continuous-flow processing using a vortex fluidic device (VFD). This involves intense micromixing a colloidal suspension of graphite in DMF and an *o*-xylene solution of C_{60} at room temperature in the absence of surfactants and other auxiliary substances. The diameters of the composite spheres, C_{60}@graphene, can be controlled with size distributions ranging from 1.5 to 3.5 μm, depending on the VFD operating parameters, including rotational speed, flow rate, relative ratio of C_{60} to graphite, and the concentration of fullerene. An electrode of the composite material has high cycle stability, with a high areal capacitance of 103.4 mF cm^{-2}, maintaining its capacitances to 24.7 F g^{-1} and 86.4 mF cm^{-2} (83.5%) at a high scan rate of 100 mV s^{-1}.

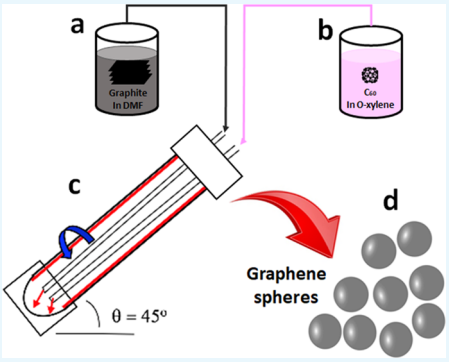

INTRODUCTION

Carbon nanomaterials have emerged as key materials for future technology, for developing complex functional structures devoid of potentially toxic metals and metals, which are likely to have supply chain issues in the near future.[1] Graphene, as a single 2D planar sheet of graphite arranged in a hexagonal lattice,[2] is one of the newest forms of such nanomaterials. It has remarkable chemical, physical, and electrical properties, with high conductivity in the absence of defects and wrinkles, large specific surface area, and excellent mechanical flexibility,[1,3] and features in a growing number of applications. These include batteries, supercapacitors, catalyst supports, drug delivery, electrode materials for energy storage devices, membranes, biomedical devices, and coatings, and these relate to its multifarious and interdisciplinary properties.[1,3−7]

Graphene can be transformed into other structures including 0D nanoparticles (carbon dots), 1D nanofibers (carbon nanofibers and nanotubes), 2D nanosheets (graphene oxide), 3D nanostructures (hollow carbon nanospheres), fullerenes, and composites of these.[8−11] Among these different carbon nanomaterials, graphene spheres show promise in a wide range of applications covering energy storage including lithium ion batteries, separation systems, oxygen-reduction, catalyst supports, nanoreactors, and adsorption.[12−21]

The synthesis of graphene spheres with smooth surfaces and uniform sizes uses soft template processing,[22] hard templating (silicon template),[23] solvothermal techniques,[24] sol pyrolysis,[25] microemulsion polymerization,[26] hydrothermal reduction,[27,28] and gelation.[29] Related to this are extended oxidation strategies to alter the morphology and surface topography of graphene oxide (GO) nanosheets, as a potential route to build up 3D graphene architectures.[30,31] However, the synthetic strategies for gaining access to such architectures are limited by the high cost of production, the use of harsh chemicals or surfactants, high temperature processing as a high-energy penalty, and limited scope for scaling up the process.[5] A challenge is to develop a scalable, low-cost method that is high in green chemistry or sustainability metrics, for gaining access to 3D graphene-based materials, including graphene spheres and composites thereof.

To this end, we have explored the use of continuous-flow processing to prepare graphene spheres and graphene-fullerene composite spheres directly from graphite and fullerene C_{60}, at room temperature, avoiding the use of auxiliary reagents. This involved the use of the in-house developed continuous-flow vortex fluidic device (VFD), which was developed early this decade.[4] It is a versatile microfluidic platform containing a dynamic thin film, in contrast to traditional channel based microfluidics, which can suffer from clogging. Mechanoenergy is delivered into the liquid in the VFD in a controlled way.[4] Under continuous-flow VFD processing, jet feeds deliver solution into an inclined rapidly rotating tube, opened at one

Received: August 18, 2019
Accepted: October 25, 2019
Published: November 7, 2019

DOI: 10.1021/acsomega.9b02656
ACS Omega 2019, 4, 19279−19286

end and usually housing a glass or quartz tube of 20 mm outside diameter (OD) and 16.000 ± 0.013 mm internal diameter (ID) (Figure 1),[32] with the liquid whirling up and out

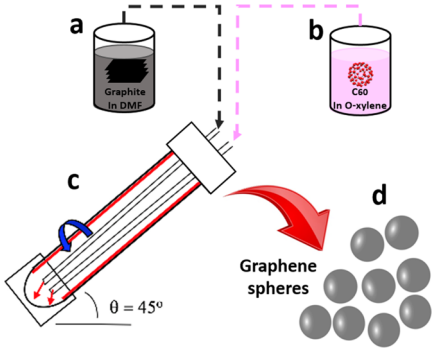

Figure 1. Schematic illustration of the overall method for fabricating the composite spheres under shear stress in a vortex fluidic device (VFD), using a 1:1 mixture of (a) an *o*-xylene solution of C_{60} and (b) a suspension of graphite in DMF, with the optimized conditions at a rotational speed (ω) = 4k rpm under continuous-flow conditions, (c) flow rate ($\dot{v}$) = 0.5 mL min^{-1}, θ = 45°, concentration of graphite in DMF 1 mg mL^{-1}, and concentration of C_{60} in *o*-xylene 0.5 mg mL^{-1}, and (d) the resulting composite spheres.

of the tube. In the confined mode of operation of the VFD, a finite volume of liquid is processed in the tube, and this is effective in processing small volumes of liquid as well as a proven method for exploring the operating parameter space of the VFD for a particular process prior to extending the process into continuous flow.[33]

The versatile VFD has a number of remarkable applications, encompassing probing the structure of self-organized systems, material processing, controlling chemical reactivity and selectivity, including enhancing enzymatic reactions, and more.[34] The first publication reporting the VFD was in 2012, describing the exfoliation of graphite along with hexagonal boron nitride, using the confined mode of operation of the device.[35] Since then, other forms of carbon have been fabricated in the device, including toroidal structures of self-assembled single walled carbon nanotubes,[36] laser aided slicing of single and multiwalled carbon nanotubes,[37] the formation of carbon dots (from multiwalled carbon nanotubes),[33] controlling the self-assembly of fullerene C_{60} molecules into nanotubules using water as an the antisolvent,[32] and the fabrication of fullerene C_{60} cones in a 1:1 mixture of *o*-xylene and DMF.[38] The VFD is also effective in controlling the nucleation and growth of palladium nanoparticles on graphene,[39] decorating palladium nanoparticles on carbon nano-onions,[40] and transforming graphene oxide into graphene oxide scrolls.[41]

We report a facile room temperature one-step synthesis of graphene spheres confining fullerene C_{60}, directly from graphite dispersed in DMF and an *o*-xylene solution of the fullerene. Remarkably, the composite material, C_{60}@graphene, is formed quantitatively with respect to graphite, with the ability to tune the size of the spheres while avoiding using auxiliary substances such as surfactants, which can affect surface properties of the resulting nanomaterials. To demonstrate an application of C_{60}@graphene, its supercapacitor performance was evaluated using the spheres as electrodes, which delivered a gravimetric capacitance of 29.5 F g^{-1} at a scan rate of 5 mV s^{-1}. While other types of graphene can reach such capacitance up to 250 F g^{-1},[42−45] the C_{60}@graphene electrode has an areal capacitance of 103.4 mF cm^{-2}, which is higher than values for other carbon derivatives, for example, in GF-CNT@Fe_2O_3 (53.56 mF/cm^2 at 10 mA/cm^2).[46] Moreover, the device reported herein can maintain its capacitances to 24.7 F g^{-1} and 86.4 mF cm^{-2} (83.5%) at a high scan rate of 100 mV s^{-1}, establishing a high rate capability of the graphene sphere electrode and potential of the material in the next-generation energy storage devices.

EXPERIMENTAL SECTION

Materials and Chemicals. Graphite flakes of 99% purity were suspended in 99.5% dimethyformamide (DMF), and fullerene C_{60} (99.5% purity) was dissolved in *o*-xylene, with both materials and solvents purchased from Sigma Aldrich.

Sample Preparation and Materials Synthesis. Suspensions of graphite in DMF were prepared at different concentrations, namely, 1, 1.5, 2, and 2.5 mg mL^{-1}, and then sonicated for 15 min followed by centrifugation for 30 min to remove undispersed graphite. Solutions of fullerene C_{60} were prepared in *o*-xylene at different concentrations, namely, 0.5, 1, 1.5, and 2 mg mL^{-1}. Initially, as-received fullerene was added to *o*-xylene, and the mixture was allowed to stand at room temperature for 24 h, whereupon it was filtered (60 μm filter paper) to remove undissolved particles before mixing with graphite dispersed in DMF in the VFD using different jet feeds (Figure 1). Operating parameter space for the VFD was systematically explored, in particular the rotational speed of the rapidly rotating glass tube, concentrations of graphite and fullerenes, flow rate, and ratio of the two solvents. After VFD processing, the resulting carbon material was collected via centrifugation at g = 1.751 rfc for 20 min.

Characterization. Samples of C_{60}@graphene on silicon wafers were prepared by drop casting followed by evaporation under ambient conditions. The morphology, size, and shape of the particles and their properties were studied using a number of complementary techniques including scanning electron microscopy (SEM) with an accelerating voltage of 5 kV, operating at 10 mm working distance, transmission electron microscopy (TEM) conducted on a TECNAI 20 microscope operated at 120 and 200 kV, and X-ray diffraction (XRD) with the data collected using a Bruker ADVANCE D8 ECO, Co Kα, at an operating wavelength of 1.7988 Å with 2θ varied from 10 to 80°. Samples of the as-prepared material were formed by drying them in nitrogen at 55 °C for 3 days. They were then stored and kept at room temperature for 48 h. Raman spectroscopy was used to confirm structure integrity of the as-prepared carbon materials, with the spectra recorded using a Horiba XploRA apparatus at a fixed wavelength of 532 nm.

Electrochemical Characterization and Supercapacitor Fabrication. To fabricate the supercapacitors, the active material was mixed with carbon black and polyvinylidene difluoride (PVDF) in a mass ratio of 80:10:10. The resulting paste was pressed and attached to platinum foils as the current collectors, between which a piece of filter paper was sandwiched as a separator and 1.0 M H_2SO_4 was used as the electrolyte. All electrochemical tests including cyclic voltammetry (CV), galvanostatic charge/discharge (CD), and electrochemical impedance spectroscopy (EIS) were carried out using a two-electrode cell configuration by a CHI 760C electrochemical workstation.

DOI: 10.1021/acsomega.9b02656
ACS Omega 2019, 4, 19279−19286

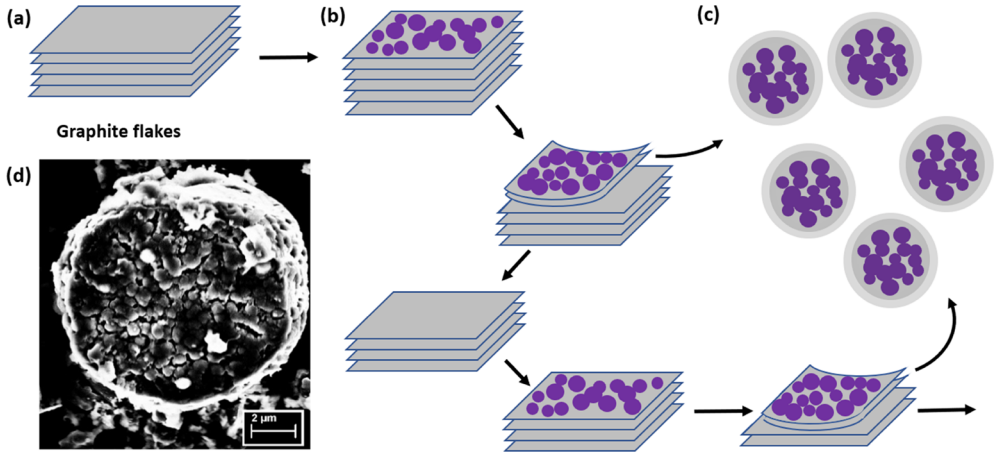

Figure 2. (a–c) Proposed mechanism of the VFD synthesis of graphene spheres confining particles of self-assembled C_{60} and (d) SEM image of a fragmented sphere formed during sonication after VFD processing; scale bar 2 μm.

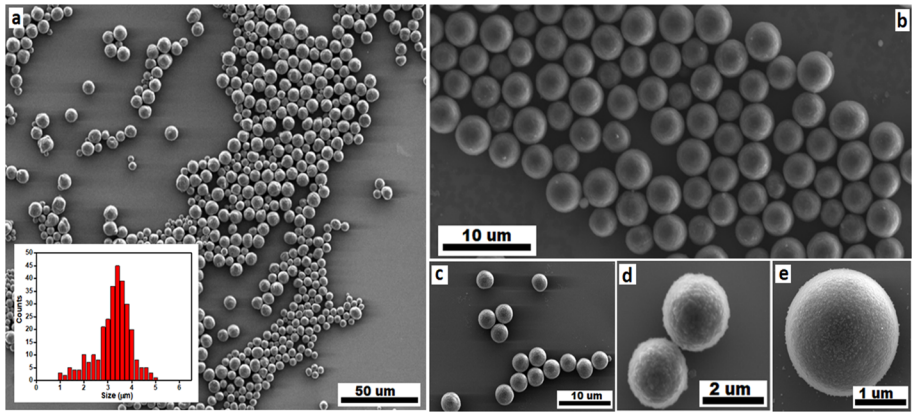

Figure 3. (a–e) SEM images (from lower magnification to higher magnification) of C_{60}@graphene, with a size distribution (inset), formed in *o*-xylene and DMF, under continuous-flow mode at a 1:1 ratio (ω = 7.5k rpm, concentration of C_{60} in *o*-xylene 0.5 mg mL^{-1}, concentration of graphite in DMF 1 mg mL^{-1}, flow rate $\dot{\nu}$ = 0.5 mL min^{-1} for both liquids entering the rotating tube in the VFD, and θ = 45°).

RESULTS AND DISCUSSION

Fabrication of C_{60}@Graphene Spheres. Conventional methods for fabricating graphene/carbon spheres require complex multistep procedures, which are typically nonscalable. We find that a graphene-fullerene C_{60} composite is readily prepared in the VFD in the absence of other reagents and importantly in quantitative yield relative to graphite with the processing illustrated in Figure 1a. Under continuous-flow mode of operation in the VFD, one jet feed delivered an *o*-xylene solution of C_{60}, with another jet feed delivering a suspension of graphite in DMF, both to the hemispherical base of the rapidly rotating glass tube. The operating parameters of the VFD were systematically varied to form the optimal product, as the most uniform in terms of morphology, size, and shape distributions of the spheres and highest yield. For this, the rotational speed was 4k rpm, the tilt angle of the glass tube θ was 45°, the concentration of C_{60} in *o*-xylene was 0.5 mg mL^{-1}, the concentration of graphite in DMF was 1 mg mL^{-1}, with a 1:1 ratio of the two solvents, and the flow rate for both liquids was 0.5 mL min^{-1}. The tilt angle of the tube in the VFD was fixed at 45°, where there is unique complex fluid dynamics, which is the optimized angle for a plethora of processing applications of the device.[4]

Mechanism of Formation of the Composite Spheres. Intense micromixing DMF with *o*-xylene in a 1:1 ratio in the

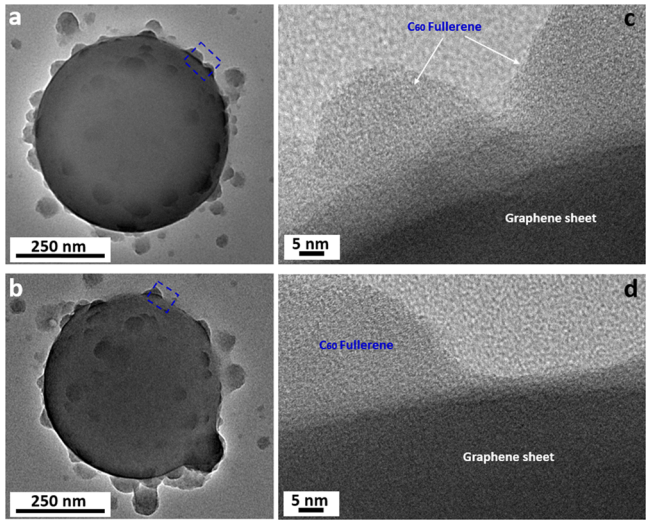

Figure 4. (a,b) TEM images of graphene spheres, (c,d) HRTEM images of graphene spheres formed in *o*-xylene and DMF, under continuous-flow mode at a 1:1 ratio at 4k rpm, concentration of fullerenes C_{60} in *o*-xylene 0.5 mg mL^{-1}, concentration of graphite in DMF 1 mg mL^{-1}, flow rate 0.5 mL min^{-1} for both liquids entering the rotating tube in the VFD, and θ = 45°.

DOI: 10.1021/acsomega.9b02656
ACS Omega 2019, 4, 19279–19286

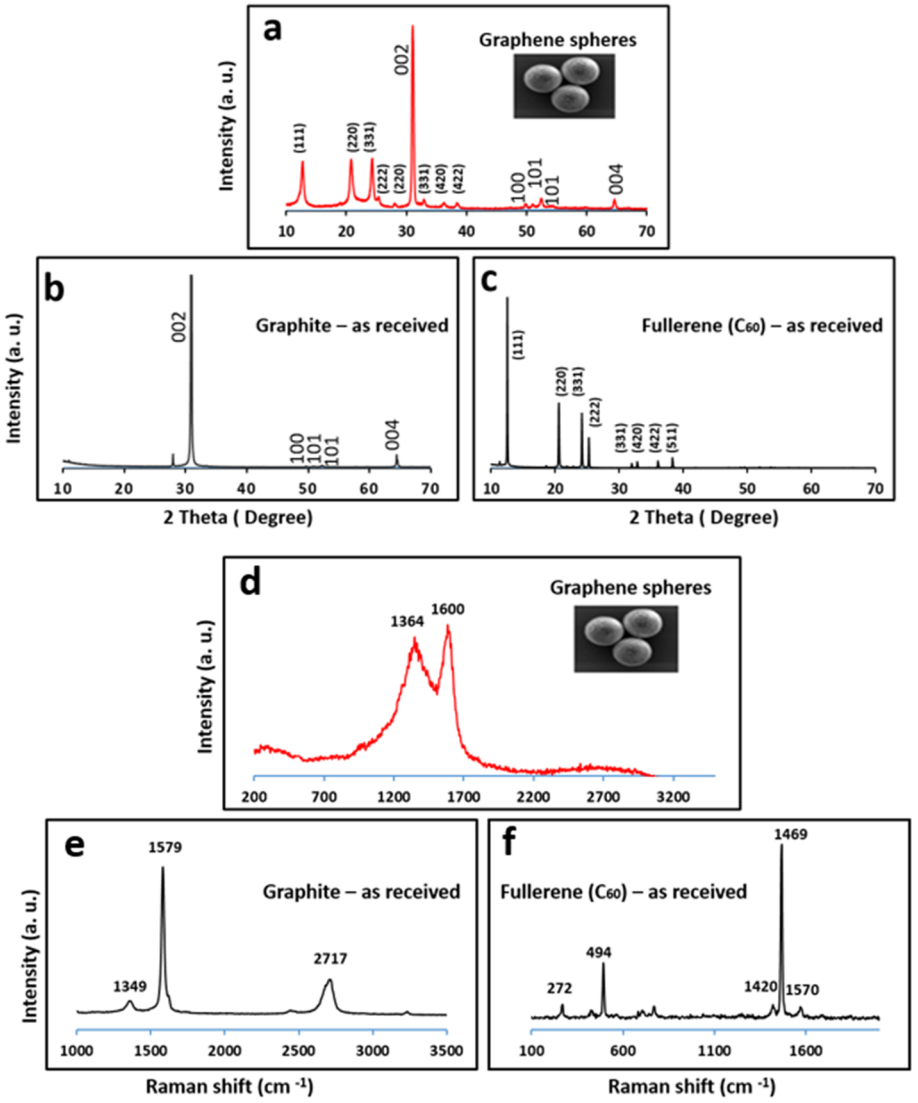

Figure 5. XRD patterns of (a) spheres prepared in the VFD, (b) graphite as-received, and (c) fullerene C_{60} as-received. Raman spectra of (d) spheres, prepared in the VFD, under continuous flow at a 1:1 ratio, 4k rpm rotational speed, concentration of fullerene 0.5 mg mL^{-1}, graphite concentration 1 mg mL^{-1}, flow rate 0.5 mL min^{-1} for both liquids, and tilt angle 45°, (e) as-received graphite, and (f) as-received C_{60}.

absence of graphite results in the formation of cones composed of approximately 0.5 to 2.5 μm diameter self-assembled particles of C_{60}, also under continuous-flow conditions and with the optimal rotational speed also at 4k rpm.[38] As in the present study, the DMF acts as an antisolvent, resulting in the formation of nanoparticles of the fullerene, which are likely to adhere to the surface of the graphite flakes (Figure 2a), facilitating exfoliation by leveraging the graphene layers, which then wrap up the fullerene particles under high shear (Figure 2b). Then the process starts again on the resulting exposed graphene surface once a certain threshold of fullerene particles adheres to the surface and so on. This accounts for the fullerene particles being primarily confined within an outer layer of graphene sheets (Figure 2c). Processing in the absence of C_{60} (for a 1:1 mixture of *o*-xylene and DMF) affords exfoliated graphene, whereas the same processing for C_{60} in the absence of graphite results in the formation of particles of the fullerene <100 nm (Figure S1), which importantly are similar to the size of the fullerene particles present within the spheres. These were determined by sonicating the isolated spheres in DMF for 30 min (Figure 2d), with the resulting ruptured spheres containing particles of C_{60} in the range of 5 to 100 nm. These findings give credence to the proposed mechanism of the formation of particles of C_{60} adhering to the exposed graphene surface of graphite, presumably favored by $\pi-\pi$ interactions between the two components. These are then transformed into spheres comprising at most a few layers of graphene, with the number of sheets of stacked graphene limited by the mechanical energy imparted in the dynamic thin film in the device.

Morphology of the C_{60}@Graphene Spheres. SEM images of different magnification of graphene sphere composites, formed under the above optimized conditions, are shown in Figure 3, along with a size distribution (inset, centered at 3.5 μm). The particles are regular spheres with smooth surfaces and are not highly aggregated. The spheres were also examined using TEM (Figure 4a,b), which revealed small particles of C_{60} ~10 to 50 nm in diameter attached to the surface of the composite materials and other nanoparticles of comparable size unattached, with C_{60} particles on the inside. The presence of C_{60} particles on the surface of the spheres and inside the spheres is in accordance with the observation by

DOI: 10.1021/acsomega.9b02656
ACS Omega 2019, 4, 19279−19286

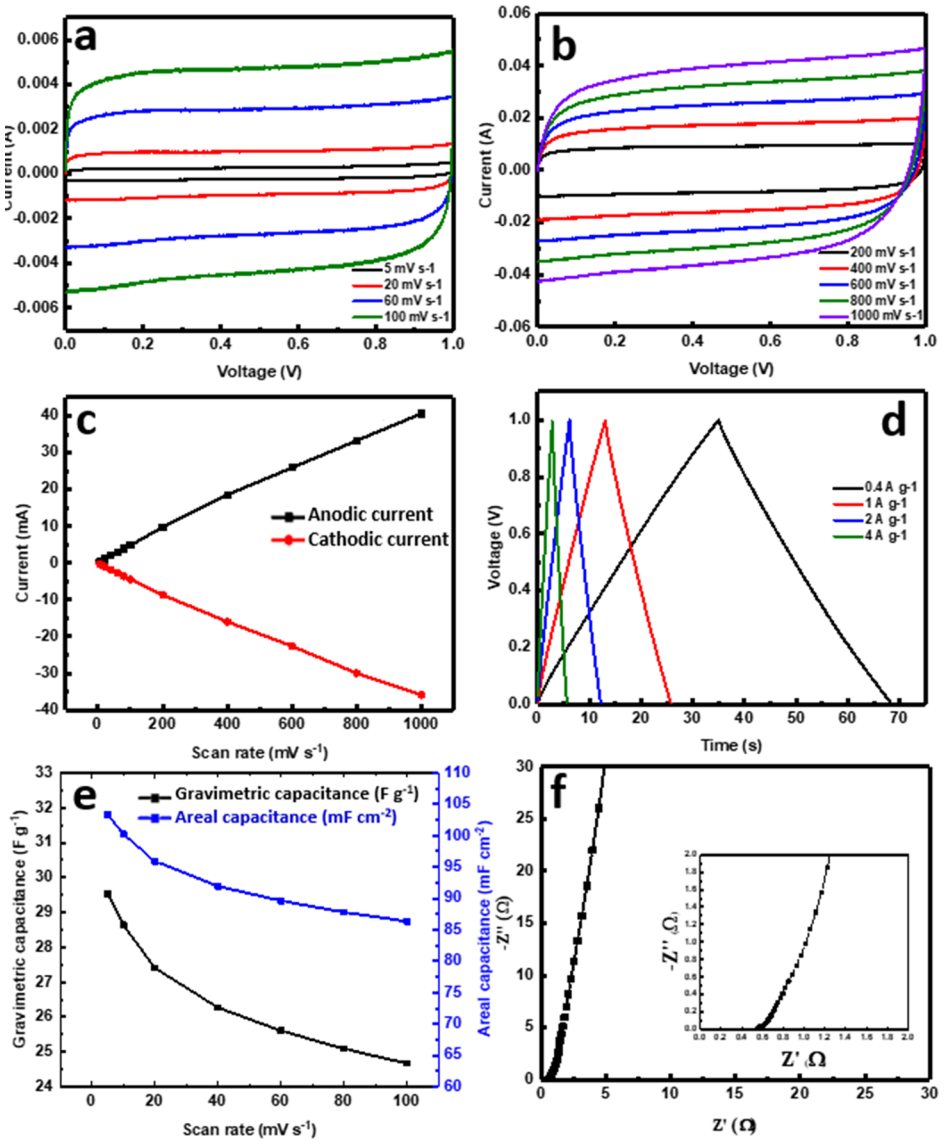

Figure 6. (a) Cyclic voltammogram (CV) curves of graphene sphere composites formed using the VFD, under continuous flow at a 1:1 ratio, 4k rpm rotational speed, concentration of fullerene 0.5 mg mL^{-1}, graphite concentration 1 mg mL^{-1}, flow rate 0.5 mL min^{-1} for both liquids, and tilt angle 45°, at different scan rates from 5 to 100 mV s^{-1}, (b) CV curves at different scan rates from 200 to 1000 mV s^{-1}, (c) response anodic and cathodic currents, (d) charge/discharge curves of graphene sphere composites at different current densities, (e) gravimetric capacitance and areal capacitance values versus scanning rate calculated from the CV curves of the graphene sphere composites, and (f) Nyquist plot of graphene sphere composites.

SEM (Figure 3). The high-resolution TEM image (Figure 4c,d) reveals that the graphene spheres have some C_{60} particles on the surface of the spheres as well as inside them.

We found that the morphology, size, and shape of the spheres varied on changing the rotational speed, flow rate of both liquids, and changing the concentrations of graphite and fullerene, as established using SEM. The optimized speed for generating smooth spheres was 4k rpm (Figure 3a–e). At much higher speed, 7.5k rpm, with the other parameters unchanged, the surfaces of the spheres are textured, but remarkably, the spheres now have a hole connecting the outer surface and inner surface of the tube (Figure S5). At 6k and 9k rpm, with the other parameters unchanged, the surfaces of the spheres are also textured and nonuniform (Figures S4 and S6). The ratio of the two solutions delivered to the VFD tube was initially set at 1:1, which was based on the success of this ratio in forming the fullerene cones[38] of comparable diameter to the spheres in the present study, the only difference being the absence of graphite. The initial flow rate of both solutions was fixed at 0.5 mL min^{-1}, which was subsequently found to be optimal. Increasing the flow rates of both solutions shuts down the formation of spheres (Figure S3). Increasing the flow rate of DMF containing graphite up to 2.5 mL min^{-1} and the flow rate of the fullerene *o*-xylene solution to 2 mL min^{-1} produced dissimilar structures, with irregular spheroidal structures (Figure S2).

XRD patterns of the spheres are consistent with the material composed of graphite/graphene and fullerene C_{60}[32] (Figure 5a–c). The spheres were collected immediately after VFD processing by centrifugation for 30 min, washed twice with hexane, and dried at 55 °C for 3 days. The major peaks of fcc fullerene C_{60} are at 2θ = 10.8, 17.7, and 20.8°, corresponding to the (111), (220), and (311), respectively, with the major peaks at 30.2, 10.8, and 60.8° corresponding to the (002) and

DOI: 10.1021/acsomega.9b02656
ACS Omega 2019, 4, 19279–19286

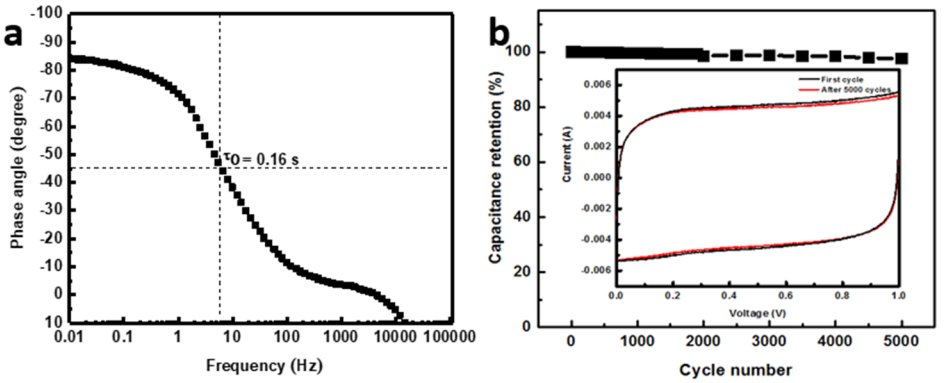

Figure 7. (a) Impedance phase angle versus frequency for a C_{60}@Graphene sphere electrode, with the material formed using the VFD, under continuous flow at a 1:1 ratio of liquids, 4k rpm rotational speed, concentration of fullerene 0.5 mg mL^{-1}, graphite concentration 1 mg mL^{-1}, flow rate 0.5 mL min^{-1} for both liquids, and tilt angle 45°. (b) Cyclic stability of the composite electrode at a scan rate of 100 mV s^{-1}; the inset is the nearly identical CV curves for first and last cycles of the electrode.

(004) planes of graphite. Clearly, the XRD data establishes the formation of a hybrid composite material composed of fcc C_{60} and graphene. From the Scherrer equation, the crystal domains of fullerenes C_{60} were estimated to be 6.5 nm in diameter. The presence of graphene as one or a limited number of stacked sheets is consistent with shifts in the graphite diffraction pattern,[47] as well as consideration of the energetics of bending a finite number of sheets, as discussed above. Moreover, the absence of some graphite peaks can be attributed to assembled fullerene C_{60} on the surface of graphene.[47] Raman spectra (532 nm excitation) for the spheres prepared at the optimized conditions and as-received graphite and fullerene C_{60} before processing, for comparison, were recorded (Figure 5d–f). Graphite itself has three main peaks, namely, the D band, G band, and 2D band, at 1349, 1579, and 2717 cm^{-1}, respectively,[48,49] and pristine C_{60} has the pentagonal pinch mode [Ag(2)] at 1469 cm^{-1} and additional Hg modes at 1420 and 1570 cm^{-1}.[50,51] In contrast, the spheres have two Raman peaks at 1364 and 1600 cm^{-1}, which can be attributed to the D band and G band, respectively, of graphene, in agreement with the literature.[50,52,53]

Electrochemical Performance. The electrochemical performance of the composite material as a symmetrical supercapacitor is summarized in Figure 6. A C_{60}@graphene electrode shows cyclic voltammetry (CV) with a nearly rectangular shape (Figure 6a), indicating an ideal capacitive behavior similar to commercial electrochemical capacitors. Figure 6a,b illustrates the CV curves at different scan rates (5 to 1000 mV s^{-1}), revealing the stability and ability of the electrode to maintain the ideal rectangular CV shapes during operation over a wide range of scan rates. The response anodic and cathodic currents (recorded from the CV curves at 0.5 V) showed a linear relationship at different scan rates (Figure 6c) with R^2 values of 0.9975 and 0.9979 for the charge and discharge curves, respectively.

The galvanostatic charge/discharge (CD) curves at different current densities (Figure 6d) show nearly triangular shapes of the CD curves due to the efficient EDLC nature of the graphene sphere electrode and fast kinetics of the electrolyte ion transport through the porous carbon electrode structure. Additionally, the low equivalent series resistance (ESR) of the fabricated device can be predicted from a small voltage drop (IR) of 0.0075 V at the start of the discharge curve measured at a current density of 1 A g^{-1}. Figure 6e displays the calculated gravimetric and areal capacitances for the graphene sphere electrode at different scan rates, delivering a gravimetric capacitance of 29.5 F g^{-1} at a scan rate of 5 mV s^{-1}, compared to different types of graphene spheres.[54] This value is lower due to the absence of residual oxygen-containing functional groups than reduced graphene oxide.[55,56] However, the graphene sphere electrode has an areal capacitance of 103.4 mF cm^{-2}, which is much higher than reported values for other carbon derivatives.[46,57] Moreover, this device can maintain its capacitances to 24.7 F g^{-1} and 86.4 mF cm^{-2} (83.5%) at a high scan rate of 100 mV s^{-1}, confirming the high rate capability of the graphene sphere electrode.

A Nyquist plot of the graphene sphere electrode (Figure 6f) shows a vertical curve at lower frequencies and no observed semicircle higher-frequency region, indicating a nearly ideal capacitive behavior of the cell. The device shows also a lower ESR of 0.5 Ω owing to the low internal resistance of the designed electrode material. The impedance phase angle versus frequency plot for the graphene sphere electrode is illustrated in Figure 7a. The device provides a phase angle of −83.8° (close to −90°) at low frequencies, showing an ideal capacitive behavior. Furthermore, the time constant τ_0 at a phase angle of −45° is found to be 0.16 s; this fast frequency response of the graphene spheres is directly related to a significant ion transport rate of the large accessible surface area of the material. The cyclic stability of the composite electrode was examined by cyclic voltammetry at a scan rate of 100 mV s^{-1} for 5000 cycles (Figure 7b), showing a capacity retention of 97.5%. The nearly identical CV curves for first and last cycles (Figure 7b, inset) confirm the good stability and high reversibility of the C_{60}@graphene electrode.

CONCLUSIONS

A simple and effective method to fabricate all carbon spheres built of fullerene C_{60} and graphene, under continuous-flow mode of operation of the VFD microfluidic platform, has been developed. The structure and the morphology of the spheres were evaluated by SEM, TEM, HRTEM, XRD, and Raman spectroscopy. The spheres are rather uniform in size and shape. Importantly, the yield of graphene spheres is high, and the processing is scalable. The method has potential for the synthesis of spheroidal composite materials of fullerenes with other 2D materials. In addition, the use of the composite material of assembled spheres in an electrochemical device and

DOI: 10.1021/acsomega.9b02656
ACS Omega 2019, 4, 19279−19286

in supercapacitance, with high capacitance maintained at a high scan rate, has potential in developing all carbon energy storage materials.

■ ASSOCIATED CONTENT

Supporting Information

The Supporting Information is available free of charge on the ACS Publications website at DOI: 10.1021/acsomega.9b02656.

Additional information on control experiments and optimizing conditions for fabricating the composite spheres (PDF)

■ AUTHOR INFORMATION

Corresponding Author

*E-mail: colin.raston@flinders.edu.au.

ORCID

Colin L. Raston: 0000-0003-4753-0079

Author Contributions

‖I.K.A. and T.M.D.A. contributed equally to this work. The manuscript was written through contributions of all authors. All authors have given approval to the final version of the manuscript.

Notes

The authors declare no competing financial interest.

■ ACKNOWLEDGMENTS

The authors gratefully acknowledge support of this work by the Australian Research Council and the Government of South Australia, the Australian Microscopy & Microanalysis Research Facility (AMMRF) at the Flinders Institute for Nanoscale Science and Technology, Flinders University, and Adelaide Microscopy. T.M.D.A would like to thank Taibah University for funding his scholarship.

■ REFERENCES

(1) Song, L.; Xin, S.; Xu, D. W.; Li, H. Q.; Cong, H. P.; Yu, S. H. Graphene-Wrapped Graphitic Carbon Hollow Spheres: Bioinspired Synthesis and Applications in Batteries and Supercapacitors. *ChemNanoMat* **2016**, *2*, 540−546.

(2) Xiang, Z.; Chen, Y.; Li, J.; Xia, X.; He, Y.; Liu, H. Submicro-sized porous SiO_2/C and SiO_2/C/graphene spheres for lithium ion batteries. *J. Solid State Electrochem.* **2017**, *21*, 2425−2432.

(3) Wu, Z.; Wang, W.; Wang, Y.; Chen, C.; Li, K.; Zhao, G.; Sun, C.; Chen, W.; Ni, L.; Diao, G. Three-dimensional graphene hollow spheres with high sulfur loading for high-performance lithium-sulfur batteries. *Electrochim. Acta* **2017**, *224*, 527−533.

(4) Britton, J.; Stubbs, K. A.; Weiss, G. A.; Raston, C. L. Vortex Fluidic Chemical Transformations. *Chem. − Eur. J.* **2017**, 13270.

(5) Chen, X.; Eggers, P. K.; Slattery, A. D.; Ogden, S. G.; Raston, C. L. Template-free assembly of three-dimensional networks of graphene hollow spheres at the water/toluene interface. *J. Colloid Interface Sci.* **2014**, *430*, 174−177.

(6) Wang, Q.; Zhang, Y.; Jiang, H.; Hu, T.; Meng, C. In situ generated $Ni_3Si_2O_5$ $(OH)_4$ on mesoporous heteroatom-enriched carbon derived from natural bamboo leaves for high-performance supercapacitors. *ACS Appl. Energy Mater.* **2018**, *1*, 3396−3409.

(7) Wang, Q.; Zhang, Y.; Jiang, H.; Meng, C. In-situ grown manganese silicate from biomass-derived heteroatom-doped porous carbon for supercapacitors with high performance. *J. Colloid Interface Sci.* **2019**, *534*, 142−155.

(8) Georgakilas, V.; Perman, J. A.; Tucek, J.; Zboril, R. Broad family of carbon nanoallotropes: classification, chemistry, and applications of fullerenes, carbon dots, nanotubes, graphene, nanodiamonds, and combined superstructures. *Chem. Rev.* **2015**, *115*, 4744−4822.

(9) Li, Z.; Liu, Z.; Sun, H.; Gao, C. Superstructured assembly of nanocarbons: fullerenes, nanotubes, and graphene. *Chem. Rev.* **2015**, *115*, 7046−7117.

(10) Yang, Z.; Ren, J.; Zhang, Z.; Chen, X.; Guan, G.; Qiu, L.; Zhang, Y.; Peng, H. Recent advancement of nanostructured carbon for energy applications. *Chem. Rev.* **2015**, *115*, 5159−5223.

(11) Cheng, Y.; Zhang, Y.; Meng, C. Template Fabrication of Amorphous Co_2SiO_4 Nanobelts/Graphene Oxide Composites with Enhanced Electrochemical Performances for Hybrid Supercapacitors. *ACS Appl. Energy Mater.* **2019**, *2*, 3830−3839.

(12) Tang, J.; Liu, J.; Torad, N. L.; Kimura, T.; Yamauchi, Y. Tailored design of functional nanoporous carbon materials toward fuel cell applications. *Nano Today* **2014**, *9*, 305−323.

(13) Meng, Y.; Gu, D.; Zhang, F.; Shi, Y.; Yang, H.; Li, Z.; Yu, C.; Tu, B.; Zhao, D. Ordered mesoporous polymers and homologous carbon frameworks: amphiphilic surfactant templating and direct transformation. *Angew. Chem., Int. Ed.* **2005**, *44*, 7053−7059.

(14) Zhang, C.; Wu, H. B.; Yuan, C.; Guo, Z.; Lou, X. W. D. Confining sulfur in double-shelled hollow carbon spheres for lithium−sulfur batteries. *Angew. Chem., Int. Ed.* **2012**, *51*, 9592−9595.

(15) Benzigar, M. R.; Joseph, S.; Baskar, A. V.; Park, D. H.; Chandra, G.; Umapathy, S.; Talapaneni, S. N.; Vinu, A. Ordered Mesoporous C_{70} with Highly Crystalline Pore Walls for Energy Applications. *Adv. Funct. Mater.* **2018**, *28*, 1803701.

(16) Paul, R.; Zhu, L.; Chen, H.; Qu, J.; Dai, L. Recent Advances in Carbon-Based Metal-Free Electrocatalysts. *Adv. Mater.* **2019**, 1806403.

(17) Liu, J.; Zhu, D.; Zheng, Y.; Vasileff, A.; Qiao, S.-Z. Self-supported earth-abundant nanoarrays as efficient and robust electrocatalysts for energy-related reactions. *ACS Catal.* **2018**, *8*, 6707−6732.

(18) Vasileff, A.; Zheng, Y.; Qiao, S. Z. Carbon Solving Carbon's Problems: Recent Progress of Nanostructured Carbon-Based Catalysts for the Electrochemical Reduction of CO_2. *Adv. Energy Mater.* **2017**, *7* (), DOI: 10.1002/aenm.201700759.

(19) Tan, H.; Li, Y.; Jiang, X.; Tang, J.; Wang, Z.; Qian, H.; Mei, P.; Malgras, V.; Bando, Y.; Yamauchi, Y. Perfectly ordered mesoporous iron-nitrogen doped carbon as highly efficient catalyst for oxygen reduction reaction in both alkaline and acidic electrolytes. *Nano Energy* **2017**, *36*, 286−294.

(20) Tan, H.; Li, Y.; Kim, J.; Takei, T.; Wang, Z.; Xu, X.; Wang, J.; Bando, Y.; Kang, Y.-M.; Tang, J.; Yamauchi, Y. Sub-50 nm Iron−Nitrogen-Doped Hollow Carbon Sphere-Encapsulated Iron Carbide Nanoparticles as Efficient Oxygen Reduction Catalysts. *Adv. Sci.* **2018**, *5*, 1800120.

(21) Zheng, J.; Zhang, Y.; Wang, Q.; Jiang, H.; Liu, Y.; Lv, T.; Meng, C. Hydrothermal encapsulation of VO 2 (A) nanorods in amorphous carbon by carbonization of glucose for energy storage devices. *Dalton Trans.* **2018**, *47*, 452−464.

(22) Caruso, F. Hollow capsule processing through colloidal templating and self-assembly. *Chem. − Eur. J.* **2000**, *6*, 413−419.

(23) Wang, Y.; Su, F.; Lee, J. Y.; Zhao, X. S. Crystalline carbon hollow spheres, crystalline carbon− SnO_2 hollow spheres, and crystalline SnO_2 hollow spheres: synthesis and performance in reversible li-ion storage. *Chem. Mater.* **2006**, *18*, 1347−1353.

(24) Zou, G.; Yu, D.; Lu, J.; Wang, D.; Jiang, C.; Qian, Y. A self-generated template route to hollow carbon nanospheres in a short time. *Solid State Commun.* **2004**, *131*, 749−752.

(25) Han, S.; Yun, Y.; Park, K. W.; Sung, Y. E.; Hyeon, T. Simple Solid-Phase Synthesis of Hollow Graphitic Nanoparticles and their Application to Direct Methanol Fuel Cell Electrodes. *Adv. Mater.* **2003**, *15*, 1922−1925.

(26) Jang, J.; Li, X. L.; Oh, J. H. Facile fabrication of polymer and carbon nanocapsules using polypyrrole core/shell nanomaterials. *Chem. Commun* **2004**, *7*, 794−795.

(27) Tang, Z.; Shen, S.; Zhuang, J.; Wang, X. Noble-metal-promoted three-dimensional macroassembly of single-layered graphene oxide. *Angew. Chem., Int. Ed.* **2010**, *122*, 4707−4711.

(28) Wang, Q.; Zhang, Y.; Jiang, H.; Li, X.; Cheng, Y.; Meng, C. Designed mesoporous hollow sphere architecture metal (Mn, Co, Ni) silicate: A potential electrode material for flexible all solid-state asymmetric supercapacitor. *Chem. Eng. J.* **2019**, *362*, 818−829.
(29) Compton, O. C.; An, Z.; Putz, K. W.; Hong, B. J.; Hauser, B. G.; Brinson, L. C.; Nguyen, S. T. Additive-free hydrogelation of graphene oxide by ultrasonication. *Carbon* **2012**, *50*, 3399−3406.
(30) Bonaccorso, F.; Lombardo, A.; Hasan, T.; Sun, Z.; Colombo, L.; Ferrari, A. C. Production and processing of graphene and 2d crystals. *Mater. Today* **2012**, *15*, 564−589.
(31) Zhang, Y.; Wang, C.; Jiang, H.; Wang, Q.; Zheng, J.; Meng, C. Cobalt-Nickel Silicate Hydroxide on Amorphous Carbon Derived from Bamboo Leaves for Hybrid Supercapacitors. *Chem. Eng. J.* **2019**, 121938.
(32) Vimalanathan, K.; Shrestha, R. G.; Zhang, Z.; Zou, J.; Nakayama, T.; Raston, C. L. Surfactant-free Fabrication of Fullerene C_{60} Nanotubules Under Shear. *Angew. Chem., Int. Ed.* **2017**, *56*, 8398−8401.
(33) Luo, X.; Al-Antaki, A. H. M.; Vimalanathan, K.; Moffatt, J.; Zheng, K.; Zou, Y.; Zou, J.; Duan, X.; Lamb, R. N.; Wang, S.; Li, Q.; Zhang, W.; Raston, C. L. Laser irradiated vortex fluidic mediated synthesis of luminescent carbon nanodots under continuous flow. *React. Chem. Eng.* **2018**, 164.
(34) Yasmin, L.; Chen, X.; Stubbs, K. A.; Raston, C. L. Optimising a vortex fluidic device for controlling chemical reactivity and selectivity. *Sci. Rep.* **2013**, *3*, 2282.
(35) Chen, X.; Dobson, J. F.; Raston, C. L. Vortex fluidic exfoliation of graphite and boron nitride. *Chem. Commun.* **2012**, *48*, 3703−3705.
(36) Vimalanathan, K.; Chen, X.; Raston, C. L. Shear induced fabrication of intertwined single walled carbon nanotube rings. *Chem. Commun.* **2014**, *50*, 11295−11298.
(37) Vimalanathan, K.; Gascooke, J. R.; Suarez-Martinez, I.; Marks, N. A.; Kumari, H.; Garvey, C. J.; Atwood, J. L.; Lawrance, W. D.; Raston, C. L. Fluid dynamic lateral slicing of high tensile strength carbon nanotubes. *Sci. Rep.* **2016**, *6*, 22865.
(38) Alsulami, I. K.; Alharbi, T. M. D.; Harvey, D. P.; Gibson, C. T.; Raston, C. L. Controlling the growth of fullerene C_{60} cones under continuous flow. *Chem. Commun.* **2018**, 7896.
(39) Goh, Y. A.; Chen, X.; Yasin, F. M.; Eggers, P. K.; Boulos, R. A.; Wang, X.; Chua, H. T.; Raston, C. L. Shear flow assisted decoration of carbon nano-onions with platinum nanoparticles. *Chem. Commun.* **2013**, *49*, 5171−5173.
(40) Yasin, F. M.; Boulos, R. A.; Hong, B. Y.; Cornejo, A.; Iyer, K. S.; Gao, L.; Chua, H. T.; Raston, C. L. Microfluidic size selective growth of palladium nano-particles on carbon nano-onions. *Chem. Commun.* **2012**, *48*, 10102−10104.
(41) Alharbi, T. M. D.; Harvey, D.; Alsulami, I. K.; Dehbari, N.; Duan, X.; Lamb, R. N.; Lawrance, W. D.; Raston, C. L. Shear stress mediated scrolling of graphene oxide. *Carbon* **2018**, 419.
(42) Ma, X.; Gan, L.; Liu, M.; Tripathi, P. K.; Zhao, Y.; Xu, Z.; Zhu, D.; Chen, L. Mesoporous size controllable carbon microspheres and their electrochemical performances for supercapacitor electrodes. *J. Mater. Chem. A* **2014**, *2*, 8407−8415.
(43) Liu, M.; Qian, J.; Zhao, Y.; Zhu, D.; Gan, L.; Chen, L. Core−shell ultramicroporous@ microporous carbon nanospheres as advanced supercapacitor electrodes. *J. Mater. Chem. A* **2015**, *3*, 11517−11526.
(44) Zhu, D.; Wang, Y.; Gan, L.; Liu, M.; Cheng, K.; Zhao, Y.; Deng, X.; Sun, D. Nitrogen-containing carbon microspheres for supercapacitor electrodes. *Electrochim. Acta* **2015**, *158*, 166−174.
(45) Zhou, J.; Lian, J.; Hou, L.; Zhang, J.; Gou, H.; Xia, M.; Zhao, Y.; Strobel, T. A.; Tao, L.; Gao, F. Ultrahigh volumetric capacitance and cyclic stability of fluorine and nitrogen co-doped carbon microspheres. *Nat. Commun.* **2015**, *6*, 8503.
(46) Zhang, X.; Lai, Y.; Ge, M.; Zheng, Y.; Zhang, K.-Q.; Lin, Z. Fibrous and flexible supercapacitors comprising hierarchical nanostructures with carbon spheres and graphene oxide nanosheets. *J. Mater. Chem. A* **2015**, *3*, 12761−12768.
(47) Zhang, K.; Zhang, Y.; Wang, S. Enhancing thermoelectric properties of organic composites through hierarchical nanostructures. *Sci. Rep.* **2013**, *3*, 3448.
(48) Kudin, K. N.; Ozbas, B.; Schniepp, H. C.; Prud'Homme, R. K.; Aksay, I. A.; Car, R. Raman spectra of graphite oxide and functionalized graphene sheets. *Nano Lett.* **2008**, *8*, 36−41.
(49) Park, J. S.; Reina, A.; Saito, R.; Kong, J.; Dresselhaus, G.; Dresselhaus, M. S. G′ band Raman spectra of single, double and triple layer graphene. *Carbon* **2009**, *47*, 1303−1310.
(50) Qu, S.; Li, M.; Xie, L.; Huang, X.; Yang, J.; Wang, N.; Yang, S. Noncovalent functionalization of graphene attaching [6, 6]-phenyl-C61-butyric acid methyl ester (PCBM) and application as electron extraction layer of polymer solar cells. *ACS Nano* **2013**, *7*, 4070−4081.
(51) Bethune, D. S.; Meijer, G.; Tang, W. C.; Rosen, H. J. The vibrational Raman spectra of purified solid films of C_{60} and C_{70}. *Chem. Phys. Lett.* **1990**, *174*, 219−222.
(52) Yu, D.; Park, K.; Durstock, M.; Dai, L. Fullerene-grafted graphene for efficient bulk heterojunction polymer photovoltaic devices. *J. Phys. Chem. Lett.* **2011**, *2*, 1113−1118.
(53) Yu, X.; Dong, Z.; Yang, J. K. W.; Wang, Q. J. Room-temperature mid-infrared photodetector in all-carbon graphene nanoribbon-C 60 hybrid nanostructure. *Optica* **2016**, *3*, 979−984.
(54) Wang, H.; Shi, L.; Yan, T.; Zhang, J.; Zhong, Q.; Zhang, D. Design of graphene-coated hollow mesoporous carbon spheres as high performance electrodes for capacitive deionization. *J. Mater. Chem. A* **2014**, *2*, 4739−4750.
(55) Moussa, M.; Zhao, Z.; El-Kady, M. F.; Liu, H.; Michelmore, A.; Kawashima, N.; Majewski, P.; Ma, J. Free-standing composite hydrogel films for superior volumetric capacitance. *J. Mater. Chem. A* **2015**, *3*, 15668−15674.
(56) Moussa, M.; El-Kady, M. F.; Abdel-Azeim, S.; Kaner, R. B.; Majewski, P.; Ma, J. Technology, Compact, flexible conducting polymer/graphene nanocomposites for supercapacitors of high volumetric energy density. *Compos. Sci. Technol.* **2018**, *160*, 50−59.
(57) Sheberla, D.; Bachman, J. C.; Elias, J. S.; Sun, C.-J.; Shao-Horn, Y.; Dincă, M. Conductive MOF electrodes for stable supercapacitors with high areal capacitance. *Nat. Mater.* **2017**, *16*, 220.

DOI: 10.1021/acsomega.9b02656
ACS Omega 2019, 4, 19279−19286